Autonomous Modification of Unstructured Environments with Found Material

Vivek Thangavelu [1*], Maíra Saboia da Silva[2*], Jiwon Choi [3] and Nils Napp[1*]

***Abstract*— The ability to autonomously modify their environment dramatically increases the capability of robots to operate in unstructured environments. We develop a specialized construction algorithm and robotic system that can autonomously build motion support structures with previously unseen objects. The approach is based on our prior work on adaptive ramp building algorithms, but it eliminates the assumption of having specialized building materials that simplify manipulation and planning for stability. Utilizing irregularly shaped stones makes the problem significantly more challenging since the outcome of individual placements is sensitive to details of contact geometry and friction, which are difficult to observe. To reuse the same high-level algorithm, we develop a new physics-based planner that explicitly considers the uncertainty produced by incomplete in-situ sensing and imprecision during pickup and placement. We demonstrate the approach on a robotic system that uses a newly developed gripper to reliably pick up stones with minimal additional sensors or complex grasp planning. The resulting system can build structures with more than 70 stones, which in turn provide traversable paths to previously inaccessible locations.**

***Index Terms*— physics simulation, autonomous construction, robotics, irregular building materials.**

I. Introduction

The social and economic need for safer, more efficient, and sustainable construction operations has motivated much ongoing research into automating construction through robotic systems [1], [2], [3]. While many of these efforts target efficiency and safety, here, we investigate the use of robotic systems for enabling novel types of construction that can be used in remote and extreme environments with insufficient access to prefabricated construction materials [4] but an abundance of irregular objects [5]. Our goal is to directly use these objects as raw construction material without any further processing. Additionally, these methods could be used for reducing the significant amount of solid construction waste [6], [7] by complementing traditional construction methods.

Robotic systems can be used to build utility structures, in which the function is more important than the exact shape, like shelter, levees, ramps [8], [9], walls or protection barrier [10], [11]. In many cases, the ability to move around in the environment is critical to allow robots to complete high-level tasks. While many methods are designed for determining or assessing areas that agents can navigate [12], [13], [14], robots with construction capabilities can modify those areas to provide mobility where needed [9], [15], [16], [17], [18]. This ability is especially important for autonomy in remote locations, where human operators are limited.

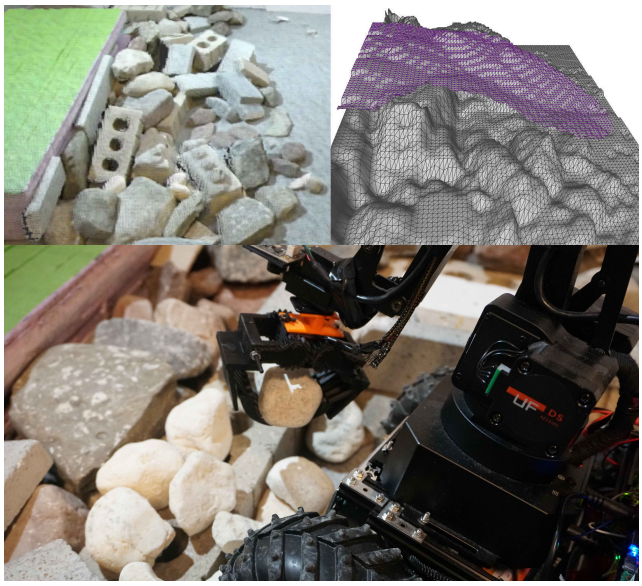

Fig. 1. (top,left) Point Cloud of Structure. (top,right) Structure mesh and the construction path (in purple). (bottom) Robot placing a stone in the structure.

In this work, we demonstrate the use of irregular objects to build utility structures in unstructured environments. We use irregularly shaped stones as a simulant material for found objects, and provide statistics of their shape descriptors in order to facilitate comparison to other materials. The robot uses these stones to build ramp-like motion support structures, which are useful not only to accomplish high-level tasks but as means to reach a goal location. In our previous results [9], [19], [20], we simulated the use of found objects by using compliant bags and rigid foam blocks. However, while these materials are convenient to manipulate and deposit, they poorly model the physical characteristics of materials that are available in real-world scenarios, like stone and concrete rubble.

Autonomous construction with stones is demonstrated to be a challenging task. Furrer et al. [21] present a system for the construction of balancing vertical towers without using mortars. The authors use a physics engine coupled with a greedy pose searching algorithm that considers structural stability to indicate the next best stone placement and is

[1]Department of Electrical and Computer Engineering, Cornell University, Ithaca, NY 14850, USA, {vs353, nnapp}@cornell.edu.

[2]Jet Propulsion Laboratory, California Institute of Technology, Pasadena, CA 14260, USA, maira.saboia.da.silva@jpl.nasa.gov.

[3]Department of Computer Science and Engineering, University at Buffalo, Buffalo, NY 14260, USA, jiwoncho@buffalo.edu.

* This project was developed while authors were affiliated to the University at Buffalo, supported by NSF#184634 and CAPES #013584/2013-08.

capable of stacking up to 4 stones per tower. By incorporating heuristics, the dry-stacking method presented by Liu et al. [11] is able to build towers of up to 6 stones. They also describe a building strategy that can build walls with 16 stones based on the approach developed for 2D irregular objects [22], which introduces a course-by-course construction approach to build dry-stacked walls grounded on heuristics form masonry manuals [23], [24], [25].

The main challenge with building 3D structures is the large action space of continuous poses for each object and the uncertainty introduced by poor contact and friction models. Unlike prior work, the proposed system uses a quick in-situ scanner to capture the stones' geometry, which compounds the geometric uncertainty further degrading the ability to simulate and predict the outcome of each action accurately. To combat these issues, we perform simulations using a rigid-body physics simulator to evaluate the effects of sensing, manipulation and motion uncertainty on the potential placement. Each simulation run is a forward simulation of a sample from a probabilistic distribution of the world model. This approach allows us to quickly rule out bad actions without spending much simulation time and estimate actions that have consistent outcomes despite the various sources of uncertainty throughout the system. The quick calculation of potentially stable placement actions represents a discretization of the action space, which is subsequently refined using a sequence of ranking methods based both on the physical object-environment interactions [22] and the construction goals of the robot [9].

The contribution of the paper is two-fold. First, we propose a physics-based deposition planner that incorporates sensing and action uncertainty for stacking irregular rigid bodies to form motion support structures. Second, an end-to-end autonomous robot system that scans stones in-situ and plans stone placements in unstructured environments to build structures that enable robot mobility. The system uses the newly developed planner as well as mechanical features such as a compliant gripper and wheel suspension to combat uncertainty. To the best of our knowledge, this is the first demonstration of an autonomous system using found stones to build functional structures in unstructured terrains, utilizing only in-situ knowledge of its environment.

A. Problem Formulation

The environment is modeled as a continuous function. The construction area Q is a bounded subset of $\mathbb{R}^2$ and domain of a bounded, non-negative height function $h : Q \rightarrow \mathbb{R}^+$ which describes a *structure*. Navigability [26] provides a method to tie robot specific kinematic constrains to the terrain model and gives a concise mathematical way to express a set of poses $\mathbf{p} \in SE(3)$ that the robot can occupy. Target volume $T_{h,u}$, for some target structure $u : Q \rightarrow \mathbb{R}^+$ with $h \leq u$, is the volume bounded between the current height of the structure h and above by u. Each object o is a rigid body described by the 3D volume it occupies, yet since measurements of its surface are noisy and incomplete, we use a shape distribution $\psi_{obj\_shape}(o)$ to describe each object o. Drawing a sample from the distribution defines a specific 3D object mesh M_o. Given a target construction volume $T_{h,u} \subset \mathbb{R}^3$ and a set of rigid objects O, the assembly process consists of n assembly steps, with each step consisting of a deposition pose $\mathbf{d}_o$ for an object $o \in O$.

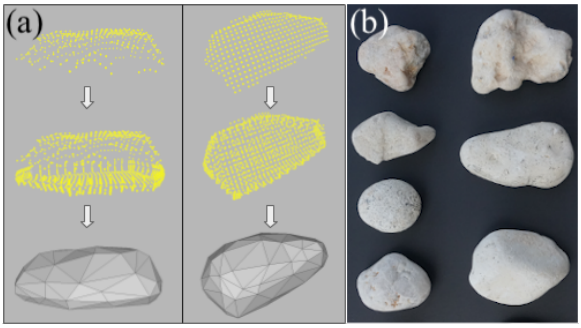

Fig. 2. (a) Sensing and internal representation of an object o. Each of the columns shows a different view of the same object. The top row shows the noisy and incomplete data from the scanning sensor. The middle and last rows showcase the augmented contour point cloud constructed using an extrusion method (Section III (b)) and the initial seed mesh, respectively. The initial seed mesh corresponds to the shape distribution $\psi_{obj\_shape}(o)$, that incorporates sensing noise. A mesh sample M_o is generated from this initial seed mesh using Monte Carlo sampling. (b) Example objects from the set O of stones used in the experiments.

The Minimal Additive Ramp Structure (MARS) [9] provides the upper bounds for the least additive construction for building *Perfect Motion Support Structures*. MARS is a monotone function that is defined to subsets of the structure domain, which in this case is called the *restricted* MARS. To build a navigable path, we potentially need to build a substructure that connects a position in the target area and the robot's initial position. By limiting the construction to only the subset of Q that minimizes the required construction volume, we identify both the target position $\mathbf{t}^*$ and the target volume $T_{h,u}$. We chose $T_{h,u}$ by exhaustively searching for the minimum restricted MARS between the robot's initial position and all points in the target area. The volume between the substructure surface and the MARS restricted to this substructure is defined as *MARS Gap*. Thus, when $T_{h,u}$ is specified by the MARS Gap, the deposition planner outputs a set of deposition poses to build a motion support structure to reach a previously inaccessible target location $\mathbf{t}^*$.

The remainder of the paper is structured as follows: §II discusses the various methods used to describe the abstract construction algorithm. §III details the system implementation, and §IV describes the experiments and the related discussions. Finally, §V concludes the paper.

II. Methods

Physics simulators at their best aim to reduce the simulation-to-reality gap by modeling various forces in the system and employing accurate shape description of the objects, estimated surface properties and the best possible physics engine parameters. However, the process of construction with found objects in unstructured environments is riddled with inaccurate and/or incomplete descriptions of the environment, especially when the agent is operating on purely in-situ knowledge. We propose a method that utilizes simulations to incorporate the uncertainties in the world

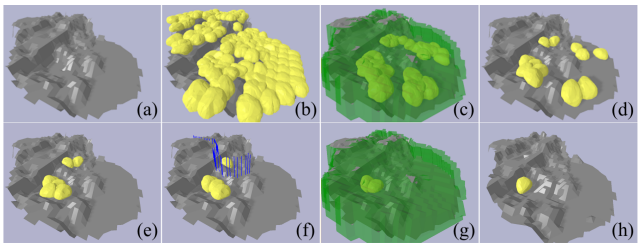

Fig. 3. Valid Pose Search and Hierarchical Filtering. (a) shows the bottom bound h of the target volume $T_{h,u}$ i.e. the substructure to build on. (b) depicts the set of physically stable poses on h. (c) depicts the initial set of valid poses $\tilde{V}$ with the upper bound u (restricted MARS bound for the substructure) shown in green. (d-h) depict the valid poses after filtering in Levels 1-5 as described in Section II-C.

description and in the robot dynamics. The physics simulator needs to be tuned to favor speed over accuracy to allow for a sufficient number of simulated samples of the world model in reasonable time (Section IV-A). In this section, we first propose the action space of deposition planning and how a physics-based simulator may be used for finding a set of physically stable poses. We then discuss how our proposed adaptive construction algorithm refines this set through an action space reduction method and picks a "good" deposition pose.

A. Action Space

The continuous action space A of an object $o \in O$ is the set of all poses $\mathbf{q} \in SE(3)$ that an object's CoM can occupy in the target volume $T_{h,u}$. Only a subset of these poses are physically stable, termed as the set of valid poses $V \subset A$.

B. Valid Pose Search

Our proposed method for a valid pose search finds an initial finite set of valid poses $\tilde{V} \subset V$, from an object shape distribution $\psi_{obj\_shape}(o)$, given a target volume $T_{h,u}$. The first step is to generate a discrete set of terrain sample points $\Delta[h]$ using a grid sampling algorithm, where $\Delta[.]$ is the discretization operator. We define the *pose initialization distribution* $\psi_{pose\_init}(\mathbf{t})$ for a point $\mathbf{t} \in \Delta[h]$ such that for every pose $\mathbf{q} \equiv \langle \mathbf{x_q}, \mathbf{r_q} \rangle \in \psi_{pose\_init}(\mathbf{t})$, $\mathbf{x_q}$ is a position at an offset along the surface normal $\mathbf{n_t}$ at $\mathbf{t}$, and $\mathbf{r_q}$ is a random rotation around $\mathbf{n_t}$.

The *Valid Pose Search* algorithm is depicted in Algorithm 1. c_{pose_inits}, $c_{mesh\_samples}$, c_{iters} and $|\Delta[h]|$ denote the number of initialization poses, object mesh samples, simulation iterations and terrain sample points, respectively. For each terrain sample point $\mathbf{t} \in \Delta[h]$ (line 2), a pose $\mathbf{q}$ is sampled from the distribution $\psi_{pose\_init}(t)$ (line 4). The object mesh $M_o \sim \psi_{obj\_shape}(o)$ is initialized with pose $\mathbf{q}$, and is pushed along the surface normal $\mathbf{n_t}$ until it touches the terrain surface (lines 6-7). We then perform forward simulation using a physics simulator to get a physically stable pose (lines 8-10), and add it to the set of valid poses if it does not intersect with the upper bound of $T_{h,u}$ (lines 11-13). We repeat lines 4-13 for new initialized poses c_{pose_inits} times per terrain point $\mathbf{t}$ for $c_{mesh\_samples}$ number of object mesh samples. Repeating lines 3-13 for every sampled mesh point gives us the initial set of valid deposition poses $\tilde{V}$. The algorithm offers a trade-off between accuracy and speed.

Algorithm 1: Valid Pose Search. Given a target volume $T_{h,u}$ and an object shape distribution $\psi_{obj\_shape}(o)$, the algorithm outputs a set of valid poses $\tilde{V}$.

```
1  Ṽ ← {}
2  for t ∈ Δ[h] do
3      for i ← 0 : c_pose_inits do
4          q ~ ψ_pose_init(t)
5          for j ← 0 : c_mesh_samples do
6              M_o ~ ψ_obj_shape(o)
7              Move M_o along the surface normal n_t until it
                is in contact with the structure
8              for k ← 0 : c_iters do
9                  Step simulation
10             end
11             if (M_o ∩ u) == φ then
12                 Ṽ ← Ṽ ∪ (Pose after simulation)
13             end
14         end
15     end
16 end
```

Large values of the constants can lead to a larger set of deposition poses for a given object on a terrain at the cost of a longer run time.

C. Action Space Reduction

We perform a hierarchical filtering to refine the set of valid poses based on various geometric, heuristic, and physics-related considerations that promote overall structural quality. At each level of the filtering algorithm, the subset of the poses that are most compliant with the specific consideration is kept. Figure 3 depicts the hierarchical filtering as part of our system implementation. The filtering levels, in order, are:

- **Level 1 - Kinematics:** This step is system-dependent and takes into account the kinematics of the robot system and eliminates poses that cannot be executed by the robot.
- **Level 2 - Distance to Target:** During the course of the construction process, the navigable area is expected to expand and shrink. When the navigable area shrinks, the set of legal actions reduces, as does the scope of strategic planning. This level promotes fewer fluctuations in the beginning stages of the construction.
- **Level 3 - Stone functionality:** Masonry building strategies associate functionality with stone shapes [24], [27]. One technique is to use larger stones in the sides, to hold the smaller inner stones in place, acting as a retaining wall, and thereby increasing the overall stability and integrity of the structure. We implement this strategy by placing stones larger than a threshold (c_{size_thres}) in locations further away from the center of the construction path, and stones smaller than the threshold in locations closer to the center of the construction path.
- **Level 4 - MARS Proximity:** We filter out poses that are closer to the upper bound as they are more likely to lead to poses that do not conform to the MARS bounds, due to various uncertainties in the system.
- **Level 5 - System Dynamics** This step is system dependent and takes into account the robot dynamics and the

Algorithm 2: Adaptive Construction Algorithm. Given a structure h, an object dataset O and a target location $\mathbf{t}^*$, the algorithm builds an access structure through a series of depositions in order to obtain a navigable path to $\mathbf{t}^*$.

1 $T_{h,u} \leftarrow MARSGap(h, \mathbf{t}^*)$
2 **while** $|T_{h,u}| > 0$ *and robot not in* $\mathbf{t}^*$ **do**
3 Pick a random object o from O
4 $F \leftarrow ValidPoseSearch(T_{h,u}, \psi_{obj\_shape})$
5 $\mathbf{d}_o \leftarrow HierarchicalFiltering(T_{h,u}, F)$
6 **if** $\mathbf{d_o} \neq \varnothing$ **then**
7 Place object o at $\mathbf{d}_o$
8 **end**
9 $T \leftarrow MARSGap(h, \mathbf{t}^*)$
10 **end**

uncertainties in the system. Each object pose is achieved by a specific robot state. We perform Monte Carlo sampling on the robot state distribution and generate $c_{dyn\_samples}$ samples, which are then simulated forward. We estimate a score for each object pose based on how probable it is for the robot state to achieve the intended object pose. This is calculated by the L2 norm of the average error in placements across all the simulated samples. The object pose with the best score is chosen as the deposition pose.

D. Adaptive Construction Algorithm

The proposed construction algorithm is depicted in Algorithm 2. Given a structure h, an abundant set of objects O to build with and a target location $\mathbf{t}^*$, the algorithm finds a series of deposition pose $\mathbf{d}_o$ for a randomly selected object $o \in O$ in each step of the assembly process to build an access structure to $\mathbf{t}^*$. The first step is to calculate the MARS Gap (line 1). The MARS bound essentially confines the action space to the least additive deposition space required to make a structure navigable. If there is space for placement (line 2), it picks a random object from the set O (line 3) and performs a *Valid Search Pose* for the given construction volume $T_{h,u}$ defined by the MARS gap (line 4). In line 5, the deposition pose is estimated using *Hierarchical Filtering* on the set of valid poses. If a deposition pose $\mathbf{d}_o$ exists (line 6), then place the object at that pose (line 7). Re-evaluate the MARS gap after placement (line 9) and continue the building process while the robot is not at $\mathbf{t}^*$.

III. System Design

A. Stone Dataset

The stone data set used in our experiments contains samples of *decorative creek* and *pebble stones* (Fig. I-A (b)), with mean length, width and height of 3.628cm, 2.764cm and 3.1cm, respectively. The distribution of the stone morphology is discussed in detail in Section IV-B.

B. Stone and Terrain Reconstruction

The system collects an angled top-view point cloud of the stones placed on the ground for the 3D shape (Fig. I-A(a)). Since the observed points is an incomplete representation of the stone, we use a filling procedure to estimate the remaining parts of the stone shape and generate an initial closed seed mesh. The contour points representing the unobserved portions of the stone are generated by an extrusion mechanism: the observed contour points are projected onto the ground plane, along with a horizontal expansion depending on the curvature of the observed points, while adding contour points along the vertical boundary (middle row in Fig. I-A (a)). This new set of points together with the observed points is a crude representation of the object. A ball pivoting surface reconstruction method is used to generate the initial seed mesh (last row in Fig. I-A (a)). A Mesh sample is generated by performing Monte Carlo sampling on the seed mesh, thus instantiating a set of contour sample points representing the stone. The closed mesh is subsequently generated by performing a surface normal estimation followed by a Poisson surface reconstruction method.

A triangular mesh of the structure is constructed from a discretized height-map of its point cloud and subsequently applying a ball-pivoting algorithm for the surface reconstruction.

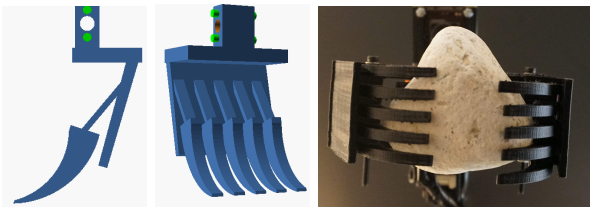

Fig. 4. (left,middle) Gripper design and (right) 3D printed gripper

C. Gripper Design

The *Stone Crabber* is a 1 DOF Pinch gripper (Fig. 4) designed to pick up stones modeled around the following restrictions: 1) small payload of the arm (300 g) and 2) in-situ 2D perception for pickup analysis. The various aspects of the gripper design are explained in the following paragraphs.

a) Grasping Motion: The gripper was designed to have an angular grasping motion in order to reduce the motion span during placements and promote picking up random geometrical objects. Four involute gears are used to drive the two-finger angular gripper.

b) Actuation: The gripper motor was selected based on the torque requirement while minimizing the weight of the motor. We chose the Robotis XL320 motor that provides a max stall torque of 0.39 N-m, weighing in at 20g.

c) Finger Design: Due to the limited gripping force, we designed the fingers to encompass the object. The fingers are curved while being flat and thin near the pick-up points in order to scoop the object. Since we are unaware of the exact 3D geometry of the object to be grasped, each finger consists of 5 parallel sub-fingers, with each sub-finger connected to the main rigid finger body through a flexure providing 1-compliant DOF. The flexure joint in each sub finger enhances compliance around the object by increasing the contact area, to help scoop the object up and increase friction after the initial grasping.

d) Fabrication: The final design of the gripper was 3D printed using ABS on a Lulzbot TAZ 6.

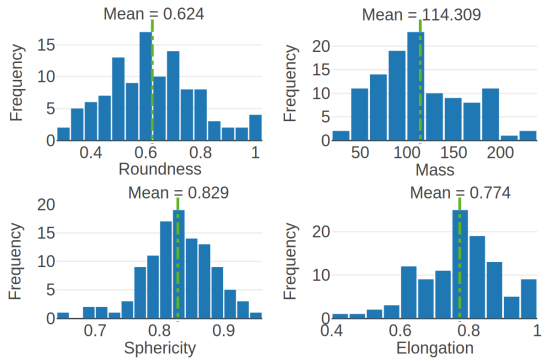

Fig. 5. Stone morphology distributions showcase the generality of the stone dataset used, and provide statistics for comparison with other datasets.

e) Control: The motor is able to provide approximate torque feedback based on the current flow. Its temperature characteristics allow it to be in a continuous grasp action of about 3 minutes until it reached its maximum operating temperature. Hence, gripper design dimensions were closely coupled to increase friction and the encompassing nature of the fingers in order to grasp a stone under minimal torque.

D. Robot Design

The robot is a low-cost mobile manipulator made from off-the-shelf components, capable of maneuvering over irregular terrain. An AprilTag [28] is mounted on top of the robot for pose estimation. A global 2D occupancy grid map is maintained for motion planning using a single overhead Kinect camera. Depth data is used to get the voxelized representation of the construction area, Q. A downward-facing VGA camera is fixed on the end-effector of the arm. It detects stones using image thresholding, and aligns the gripper along a stone's major axis using visual servoing during pickup. We present a more detailed description of the robot design and the construction system in [19].

IV. Experiments and Discussions

A. Modeling Uncertainties and System Parameters

We use pybullet [29] for rigid body physics simulations. In pybullet, the controllable parameters are given by the tuple $(c_{sim\_time}, c_{iters}, c_{max\_faces})$, where c_{sim_time} is the simulation time step, c_{iters} is the number of forward simulation steps and c_{max_faces} is the number of maximum vertex faces in our object representations.

For a given input to *ValidPoseSearch*, we perform parameter tuning by comparing the algorithm's performance and run times of the best possible setting ($(0.004, 2000, 1500)$ with a mean run time of 58s) in the coordinate space with other possible tuples. This is done by matching each pose before and after simulation and then calculating the error in position and orientation between the simulated poses. We then calculate the mean error and variance in position and orientation across all such poses. Smaller c_{sim_time}, larger c_{iters} and larger c_{max_faces} favor accuracy over speed. We perform a multi-level search by keeping two parameters constant, while comparing against different values of the third parameter. Our parameter tuning favors speed and generality over accuracy and chooses a value that does not deviate greatly from the best setting for much lower run times. The selected parameters are $(0.09, 300, 250)$ with a mean run time of 9s.

For a reasonable construction time based on our system specification, we set the number of pose initializations c_{pose_inits} to 3. The overhead camera was positioned at 1.5m from the stone pick area, looking at them at an angle of $-30°$ from the camera z plane. Given the relatively small stone dimensions, the number of sample points per stone was less than 100. Taking into account the physics engine performance, the maximum number of mesh faces c_{max_faces} for each stone was set to 250 by performing a quadric based edge collapse strategy for mesh simplification [30]. Using the specified object shape distribution, the variations in the mesh shape between different samples after mesh simplification were unnoticeable for a $c_{iters} = 300$. Hence, $c_{mesh\_samples}$ was set to 1. The masses of various objects were estimated using the mean stone density value of dolomite stones ($2.3\mathrm{g}/\mathrm{cm}^3$). A safe operating payload range for the arm after the gripper installation was 200g; the size threshold for stones c_{size_thres} was set to at half this value, 100g.

We utilized a desktop with the following configuration for running the simulations and adaptive construction algorithm: Intel Core(TM) i7-6700 CPU @ 3.40GHz and 16GB DDR3 RAM. With these settings, the average run time of our physics simulations for one assembly step was around 20s.

B. Stone Dataset Distribution

Although we use only in situ knowledge to plan for depositions, and the stones used in our experiments mimic the ones found in real-world scenarios, we present the characteristics of our stone dataset (Fig. 5) in order to exhibit the extent of our system in the general sense of construction with stones. For example, the stone morphology distribution can be used to compare our dataset with that of stones found on mars [5].

There are many quantitative characteristics to describe the morphology of sedimentary rocks [5]. Here, we elucidate the exact methods used to describe the morphology of our stone dataset. The stone morphological properties were semi-autonomously calculated from 2D images of the stones.

1) Elongation[31]: It measures the projection of the stone and is given by $E = W/L$. The length (L) and width (W) of the stone are given by the major and minor axes, respectively.

2) Sphericity[32]: It is a three-dimensional property that can be estimated from a 2D image of a stone and is a measure of how spherical the stone is. It is given by $S = (D_i/D_c)^{0.5}$, where D_i and D_c are the diameters of the largest inscribed and smallest circumscribing circles, respectively.

3) Roundness[33]: It is a two-dimensional property that measures the relative curvature of the stone's cross-section $R = r_s/D_i$, where r_s is the radius of the smallest corner. The stone face that best describes the relative curvature of the stone was chosen during the scanning process.

C. Experimental Setup

The setup consists of a target area, shown in green (Fig. 6), that is initially inaccessible. The robot is deployed on a

TABLE I
EXPERIMENTS

Exp ID	Depositions		Failed Pickups	Failed Depo-sitions	Target Height (cm)	Goal Reached
	Count	Total Weight (kg)				
1	72	7	2	2	13	Yes
2	44	4.37	1	4	13	Yes
3	74	7.2	1	6	18	No
4	45	4.028	2	2	13	Yes
5	21	1.691	3	2	13	Yes

terrain that is navigable and has access to an abundant supply of stones from a specified region (quarry). The robot system is tasked to build a navigable path to the target area using the stones from the quarry. Starting from the largest stone option, the robot estimates a deposition pose. If no pose was found, it either: (a) moves to the next largest stone until it finds a stone with a valid deposition pose, or (b) requests for more options. Once the building process is completed, the robot finds a navigable path in the structure and attempts to reach the target area. In the experiments, the robot's sensing range is large enough to see the target structure.

Each trial experiment (Table I) consists of a distinct initial irregular terrain. In each assembly step, the robot autonomously navigates to the quarry, plans a deposition pose, picks up the stone and deposits it on the structure. This is repeated until the robot eventually builds, and autonomously detects and climbs the navigable structure. Unless specifically mentioned, manual interventions to the entire building process are limited to battery replacements in the rover. Apart from the motion planning algorithm, the simulation, meshing and perception algorithms run on an external computer.

Experiment 1: The structure was initialized with an unstructured terrain. The target height was 13cm from the ground plane and the robot used stones from the quarry to autonomously build and navigate a path to the target location.

Experiment 2: The structure was initialized with a different unstructured terrain (Fig. 6 (a)). A navigable path was built using 44 stones weighing a total of 4.37kg.

Experiment 3: The structure has a different initial terrain and a higher target location than the previous runs (Fig. 6 (b)). However, it consisted of features if taken advantage of, can help the robot system to build a navigable path with lesser material. A part of the structure consists of a small ramp followed by a pit that the rover had to fill to move to the target location. After the structure was deemed complete, the robot while autonomously navigating through the terrain flipped due to a motion planning uncertainty. The structure was however climbable when operated manually.

Experiment 4: The structure was initialized with a large flat ground. The rover had to build a ramp on a much smoother surface without any supporting structures in the side, to help hold the built structure in place. Hence, as the rover builds the ramp and beings to use it, stones started to move outwards. The robot had to compensate for the reduction in ramp volume by building larger structures to sustain the robot's weight.

Experiment 5: The structure is similar to the previous experiment except for the presence of supporting structures in the side and a more uneven terrain that can give rise to better stone depositions, stability due to increased friction and possible interlocking. The robot was able to build the structure with lesser material to get to the target location.

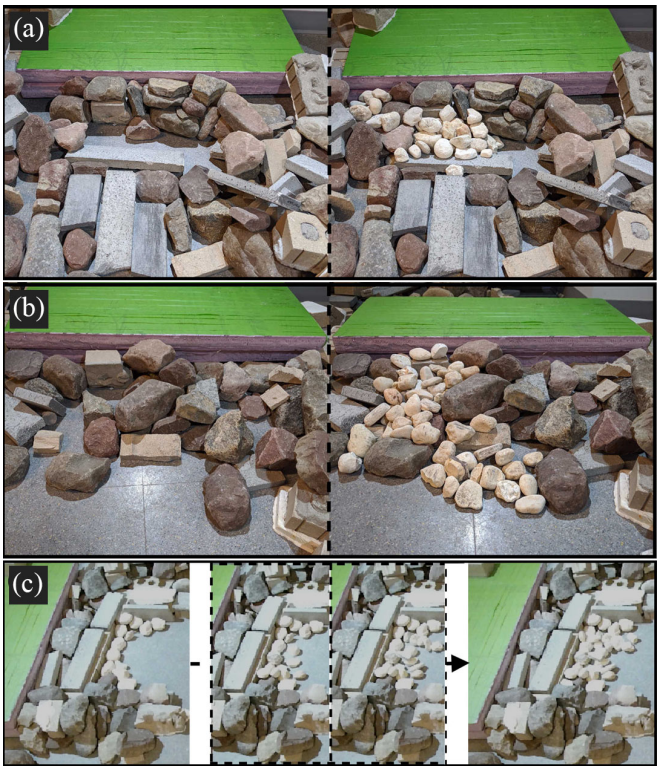

Fig. 6. Experiments. (a) and (b) depict the the before (left column) and after (right column) scenarios in experiment runs 2 and 3, respectively. (c) depicts the before, intermediate and after scenarios for run 5. Video of the experiments can be found in shorturl.at/stJK8.

V. CONCLUSION

The presented system is able to build navigable structures over unstructured terrain with found stones without prior knowledge of either the stones or the environment. The system can operate fully autonomously over many hours and find, choose, and deposit stones to build motion support structures. The adaptive construction algorithm is robust to uncertainties in the environment and found building material by estimating the prediction quality of the embedded physics simulation when choosing the next deposition. The experimental runs show various unstructured scenarios where the robot system was able to utilize the adaptive construction algorithm to reach its target location.

In future works, we aim to study the stability of each deposition pose and how it contributes to the overall stability of the structure. We would also like to study, in a more controlled environment, the deviation between the intended deposition pose and the actual final pose after deposition. This would allow us to better model the environment, and understand the relationship between various parameters of physics simulation and the complexity of the environment.

ACKNOWLEDGMENT

This project was developed while authors were affiliated to the University at Buffalo, supported by NSF184634 and CAPES 013584/2013-08.

REFERENCES

[1] K. H. Petersen, N. Napp, R. Stuart-Smith, D. Rus, and M. Kovac, "A review of collective robotic construction," *Science Robotics*, vol. 4, no. 28, 2019.

[2] M. K. Heinrich, S. von Mammen, D. N. Hofstadler, M. Wahby, P. Zahadat, T. Skrzypczak, M. D. Soorati, R. Krela, W. Kwiatkowski, T. Schmickl *et al.*, "Constructing living buildings: a review of relevant technologies for a novel application of biohybrid robotics," *Journal of the Royal Society Interface*, vol. 16, no. 156, p. 20190238, 2019.

[3] H. Ardiny, S. Witwicki, and F. Mondada, "Are autonomous mobile robots able to take over construction? a review," *International Journal of Robotics, Theory and Applications*, vol. 4, no. 3, pp. 10–21, 2015.

[4] G. B. Sanders and W. E. Larson, "Progress Made in Lunar In Situ Resource Utilization under NASA's Exploration Technology and Development Program," *Journal of Aerospace Engineering*, vol. 26, no. 1, pp. 5–17, 2013.

[5] R. A. Yingst, A. Haldemann, K. L. Biedermann, and A. M. Monhead, "Quantitative morphology of rocks at the mars pathfinder landing site," *Journal of Geophysical Research: Planets*, vol. 112, no. E6, 2007.

[6] USEPA, "Advancing sustainable materials management: 2014 fact sheet," *United States Environmental Protection Agency, Office of Land and Emergency Management, Washington, DC 20460*, no. November, p. 22, 2016.

[7] P. Eversmann, "Robotic fabrication techniques for material of unknown geometry," in *Humanizing Digital Reality*. Springer, 2018, pp. 311–322.

[8] N.Napp and R.Nagpal, "Robotic construction of arbitrary shapes with amorphous materials," in *Robotics and Automation (ICRA), 2014 IEEE International Conference on*. IEEE, 2014, pp. 438–444.

[9] M. Saboia, V. Thangavelu, and N. Napp, "Autonomous multi-material construction with a heterogeneous robot team," *Robotics and Autonomous Systems*, 2019.

[10] N. Melenbrink and J. Werfel, "Autonomous sheet pile driving robots for soil stabilization," in *Proceedings of the IEEE International Conference on Robotics and Automation*. IEEE, 2019.

[11] Y. Liu, J. Choi, and N. Napp, "Planning for robotic dry stacking with irregular stones," in *Field and Service Robotics*. Springer, 2019.

[12] Y. Tanaka, Y. Ji, A. Yamashita, and H. Asama, "Fuzzy based traversability analysis for a mobile robot on rough terrain," in *2015 IEEE International Conference on Robotics and Automation (ICRA)*. IEEE, 2015, pp. 3965–3970.

[13] L. Wellhausen, A. Dosovitskiy, R. Ranftl, K. Walas, C. Cadena, and M. Hutter, "Where should i walk? predicting terrain properties from images via self-supervised learning," *IEEE Robotics and Automation Letters*, vol. 4, no. 2, pp. 1509–1516, 2019.

[14] X. Meng, Z. Cao, S. Liang, L. Pang, S. Wang, and C. Zhou, "A terrain description method for traversability analysis based on elevation grid map," *International Journal of Advanced Robotic Systems*, vol. 15, no. 1, p. 1729881417751530, 2018.

[15] T. Tosun, C. Sung, C. McCloskey, and M. Yim, "Optimal structure synthesis for environment augmenting robots," *IEEE Robotics and Automation Letters*, vol. 4, no. 2, pp. 1069–1076, 2019.

[16] N. Napp and R. Nagpal, "Distributed amorphous ramp construction in unstructured environments," *Robotica*, vol. 32, no. 2, pp. 279–290, 2014.

[17] N. Melenbrink, P. Michalatos, P. Kassabian, and J. Werfel, "Using local force measurements to guide construction by distributed climbing robots," *In Proceedings of IEEE/RSJ international conference on intelligent robots and systems (IROS)*, 2017.

[18] R. Fujisawa, N. Nagaya, S. Okazaki, R. Sato, Y. Ikemoto, and S. Dobata, "Active modification of the environment by a robot with construction abilities," *ROBOMECH Journal*, vol. 2, no. 1, p. 9, Apr 2015.

[19] M. Saboia, V. Thangavelu, W. Gosrich, and N. Napp, "Autonomous adaptive modification of unstructured environments," *Proc. Robotics: Science & Systems XIV (RSS 2018)*, 2018.

[20] M. Saboia, V. Thangavelu, and N. Napp, "Autonomous multi-material construction with a heterogeneous robot team," in *Distributed Autonomous Robotic Systems*. Springer, 2018.

[21] F. Furrer, M. Wermelinger, H. Yoshida, F. Gramazio, M. Kohler, R. Siegwart, and M. Hutter, "Autonomous robotic stone stacking with online next best object target pose planning," in *2017 IEEE International Conference on Robotics and Automation (ICRA)*. IEEE, 2017, pp. 2350–2356.

[22] V. Thangavelu, Y. Liu, M. Saboia Da Silva, and N. Napp, "Dry stacking for automated construction with irregular objects," in *2018 IEEE International Conference on Robotics and Automation (ICRA)*. IEEE, 2018.

[23] K. Gardner, *Stone Building*. The Countryman Press, 2017.

[24] C. McRaven, *Building stone walls*. Storey Publishing, 1999, vol. 217.

[25] J. Vivian, *Building stone walls*. Storey Publishing, 2014.

[26] N. Napp and R. Nagpal, "Distributed Amorphous Ramp Construction in Unstructured Environments." [Online]. Available: https://www.cse.buffalo.edu//~nnapp/papers/new.pdf

[27] J. Vivian, *Building Stone Walls*. Storey Publishing, 1976.

[28] E. Olson, "Apriltag: A robust and flexible visual fiducial system," in *2011 IEEE International Conference on Robotics and Automation (ICRA)*. IEEE, 2011, pp. 3400–3407.

[29] E. Coumans and Y. Bai, "Pybullet, a python module for physics simulation for games, robotics and machine learning," *GitHub repository*, 2016.

[30] M. Zhou and M. Y. Wang, "Engineered model simplification for simulation based structural design," *Computer-Aided Design and Applications*, vol. 9, no. 1, pp. 87–94, 2012.

[31] E. Dapples and J. Rominger, "Orientation analysis of fine-grained clastic sediments: a report of progress," *The Journal of Geology*, vol. 53, no. 4, pp. 246–261, 1945.

[32] N. A. Riley, "Projection sphericity," *Journal of Sedimentary Research*, vol. 11, no. 2, pp. 94–95, 1941.

[33] J. E. Dobkins and R. L. Folk, "Shape development on tahiti-nui," *Journal of Sedimentary Research*, vol. 40, no. 4, pp. 1167–1203, 1970.